Longitudinal Imaging Biomarkers Correlate with Progressive Motor Deficit in the Mouse Model of Charlevoix-Saguenay Ataxia

Valentina Gigliucci,[1] Su-Chun Huang,[2] Giorgio Boschetti,[1,3] Alessandra Scaravilli [ID],[4] Valerio Castoldi,[2] Paola Podini,[5] Angelo Quattrini,[5] Sirio Cocozza [ID],[4] Letizia Leocani [ID],[2,3] and Francesca Maltecca [ID] [twitter][1,3]

Objective: In autosomal recessive spastic ataxia of Charlevoix-Saguenay (ARSACS) disease, severity and age of onset vary greatly, hindering to objectively measure and predict clinical progression. Thickening of the retinal nerve fiber layer is distinctive of ARSACS patients, as assessed by optical coherence tomography, whereas conventional brain magnetic resonance imaging findings include both supratentorial and infratentorial changes. Because longitudinal imaging studies in ARSACS patients are not available to define these changes as biomarkers of disease progression, we aimed to address this issue in the ARSACS mouse model.

Methods: We performed longitudinal retinal OCT and brain MRI in the $Sacs^{-/-}$ ARSACS mouse model, alongside motor and coordination assessment in the beam walking test. We also investigated visual function and the molecular mechanisms underlying RNFL increased thickness by histology and immunofluorescence.

Results: We demonstrated that RNFL thickening by OCT gradually increases in the early stages of pathology in the $Sacs^{-/-}$ mouse model, reflecting the progression of motor impairment, and later reaches a plateau when thinning of the posterior corpus callosum becomes detectable by MRI. Mechanistically, we unveiled that RNFL thickening is associated with aberrant accumulation of non-phosphorylated neurofilament H and glial fibrillary acidic protein. We also uncovered mild signs of myelin pathology coherent with increased latency of visual evoked potentials, and altered retinal activation by photopic electroretinography.

Interpretation: We show that both RNFL thickening and MRI changes may represent biomarkers of disease progression in the $Sacs^{-/-}$ mouse model. Our data gathers knowledge instrumental to clinical studies, holding potential as readout for treatment efficacy.

ANN NEUROL 2024;00:1–10

Autosomal recessive spastic ataxia of Charlevoix-Saguenay (ARSACS)[1,2] (OMIM 270550) is caused by mutations in the *SACS* gene[3] encoding for sacsin, a huge protein mostly expressed in the central nervous system, particularly in the Purkinje cells (PCs) of the cerebellum.[4] Abnormal vimentin remodeling in ARSACS patients' fibroblasts,[5] as well as neurofilament (NF) bundling in neurons from ARSACS patients' postmortem samples and mouse

models[4,6–8] indicate that sacsin regulates intermediate filament assembly.

The variability in symptomatology and age of onset[2,3] makes it difficult to objectively evaluate and predict pathology progression in ARSACS patients. Few longitudinal studies have been performed[9,10] and biomarkers of disease progression have not yet been identified. Reliable and standardized biological features that could be non-invasively assessed over time are, therefore, strongly needed for better diagnosis, monitoring of pathology course and for treatment design.

Most ARSACS patients present a characteristic thickening of the retinal nerve fiber layer (RNFL), as visualized by optical coherence tomography (OCT).[11,12] The RNFL contains the unmyelinated axons of the retinal ganglion cells (RGCs), which converge to form the optic nerve.[13] RNFL thickening is a hallmark of pathology to discriminate ARSACS among other types of ataxias.[11,12] Interestingly, it does not cause evident visual impairment in patients, and it is unknown if ARSACS patients are born with this peculiar feature. Whether RNFL thickening could be used as a readout for disease progression in ARSACS is still debated, because no systematic longitudinal OCT study has been performed so far, and the molecular causes underlying such thickening are unknown.

Among the different magnetic resonance imaging (MRI) changes reported in ARSACS patients via conventional brain scans,[14] the most consistent finding is a "bulky" appearance of the pons, coupled to a selective atrophy of the superior portion of the cerebellar vermis.[15] Supratentorial involvement has been sporadically described (ie, cerebrum atrophy, with a more prominent involvement of parietal regions,[1] and thinning of the *corpus callosum*[16]), although no information about its change over time is available.

Sacs$^{-/-}$ mice recapitulate the ARSACS motor impairments and cerebellar PCs degeneration,[6] however, it has never been explored if these mice also recapitulate the retinal alterations found in ARSACS patients.

A single cell RNA-sequencing study in human retina reports that *SACS* is expressed in RGCs, horizontal cells, amacrine cells, bipolar cells, and Müller glia.[17] In the mouse retina, *Sacs* transcript pattern is similar, with the exception of Müller glia where *Sacs* is not expressed.[18,19] This evidence strongly suggests that NF dynamics could be altered also in RGCs.

Here, we present a longitudinal OCT in vivo characterization of RNFL thickening in *Sacs*$^{-/-}$ mice and its correlation with motor impairment. We demonstrate that RNFL thickening can represent a biomarker to monitor progression at early stages of pathology in the *Sacs*$^{-/-}$ mice, whereas alteration of the corpus callosum by MRI

brain scan could be useful at later stages. Finally, we also dissect the molecular mechanisms leading to the selective increase in RNFL thickness in ARSACS.

Materials and Methods

Animals
All experimental procedures were performed in accordance with experimental protocols approved by the IACUC 1195 of San Raffaele Scientific Institute on both male and female *Sacs*$^{-/-}$ mice[6] and controls.

OCT Scanning
Mice underwent bilateral circle scans with a Micron IV Image-Guided OCT for rodents (Phoenix Research Labs; Pleasanton, CA). Using the optic nerve head (ONH) as anatomical marker, images were acquired in the following regions: nasal superior (region 1), temporal superior (region 2), nasal inferior (region 3), and temporal inferior (region 4). At each zone, 3 circle scans with a diameter of 542μm were acquired. Every circle scan was averaged from 50 B-scans, whereas every B scan was composed by 1,024 A-scans with the axial resolution of 2.2μm.

Beam Walking Test
Balance and motor coordination were assessed in the beam walking (BW) test as we previously described[8] (Data S1).

MRI Scan and Analysis
All MRI studies were performed on a 7-T Preclinical Scanner (BioSpec 70/30 USR, Paravision 6.0.1; Bruker, Billerica, MA). All information is provided in Data S1.

Eyes Collection and Paraffin Embedding
Eyes were fixed for 24 hour in Davidson's solution (0.74% formaldehyde, 35% ethyl alcohol or ethanol [EtOH], 10% acetic acid in H_2O), and moved to EtOH 70%. Samples were gradually dehydrated and embedded in paraffin, cut on a microtome collecting 3μm-thick slices at planes where the optic nerve was present.

Histochemical Staining and Analysis
Retinal slices were stained with hematoxylin–eosin (H&E) and scanned at $40\times$ with a slide scanner (Leica, Wetzlar, Germany). RGC count and RNFL thickness measure were performed with Aperio ImageScope (Leica).

Visual Evoked Potential and Photopic Electroretinogram
For each mouse, visual evoked potential (VEP) and photopic electroretinogram (pERG) were recorded consecutively in a unique session. Non-invasive epidermal VEPs were recorded, as described previously[20,21] (see Data S1).

pERG was recorded from 1 eye at a time using a corneal electrode connected via flexible cables to a Micromed amplifier, as reported previously.[20,21]

A

OCT — Beam walking — 1 month

OCT — Beam walking — MRI — 3 months

OCT — Beam walking — 5 months

OCT — Beam walking — VEP, ERG — 7 months

OCT — MRI — VEP, ERG — Tissue collection — 9 months

B

Region2 (**R2**): temporal superior

Optic nerve head (ONH)

RE

Scanning orientation: counterclockwise, started from 315°

Region1 (**R1**): nasal superior

Region4 (**R4**): temporal inferior

Region3 (**R3**): nasal inferior

C

OCT scan

R1 — $Sacs^{+/+}$ — $Sacs^{-/-}$

R2

R3 — *** *** **** ****

R4 — ** **** ** ***

RNFL thickness (μm): 12, 14, 16, 18, 20, 22 at 1 mo, 3 mo, 5 mo, 7 mo, 9 mo

D

Beam walking

Latency to cross

$Sacs^{+/+}$ — $Sacs^{-/-}$

Latency (s): 0, 5, 10, 15 at 1 mo, 3 mo, 5 mo — ns * ***

$Sacs^{+/+}$ — $Sacs^{-/-}$

Latency (s): 25, 20, 15, 10, 5 — Males ** — Females * — *

7 mo

Missteps

$Sacs^{+/+}$ — $Sacs^{-/-}$

Num. of Missteps (Avg./run): 2, 4, 6 at 1 mo, 3 mo, 5 mo — ns * ****

$Sacs^{+/+}$ — $Sacs^{-/-}$

Missteps (avg. n./run): 25, 20, 15, 10, 5 — Males **** — Females * — **

7 mo

(Figure legend continues on next page.)

Immunofluorescence Staining

Retinal slices were deparaffinized, rehydrated, and standard immunofluorescence (IF) conditions were used.[8] Primary antibodies: non-phosphorylated NFH (npNFH) 1:150 (SMI32; Biolegend, San Diego, CA, 801701) and glial fibrillary acidic protein (GFAP) 1:500 (Dako, Glostrup, Denmark, Z0334). Secondary antibodies: goat-anti-mouse-AF488 1:500 (Invitrogen, Waltham, MA, A-11001), goat-anti-rabbit-AF546 1:500 (Invitrogen, A-11035). Images were acquired with an Olympus FluoVIEW FV3000RS Confocal microscope, 60× magnification, and stitching was generated with Arivis software (Zeiss, Oberkochen, Germany) (see Data S1 Supplementary Methods for analysis).

Western Blot on the Retina and Antibodies

The retinas were lysed in a 1% Triton containing-buffer[8] and dissociated by sonication followed by Dounce homogenization. The following antibodies were used: anti-NFH (Millipore, Burlington MA, AB1989), GFAP (Dako, Z0334), cellular retinaldehyde binding protein (CRALBP) (Santa Cruz Biotech, Dallas, TX, sc-59487), and calnexin (Sigma-Aldrich, St. Louis, MO, Merck KGaA, C4731). Secondary antibodies included horseradish peroxidase (HRP)-conjugated anti-mouse and anti-rabbit immunoglobulin G (GE Healthcare, Issaquah, WA).

Electron Microscopy

Optic nerves were collected and postfixed as previously described.[8] Electron microscope (EM) magnification was set at 15,000×; (Leo 912 Omega). G-ratio of the optic nerve axons was calculated as axoplasmic diameter/total axon diameter (Fiji software).

Statistical Analyses

Statistical analyses were calculated with GraphPad 8 (https://www.graphpad.com/scientific-software/prism/). Statistical tests for each experiment are indicated in the Figure legends.

Results

RNFL Thickness in Sacs$^{-/-}$ Mice Increases during the First Months, Mirroring Motor Impairment

Because of the lack of longitudinal studies in ARSACS patients, we used the Sacs$^{-/-}$ mouse model to investigate if RNFL thickening could represent a valuable marker of disease progression. We first performed OCT scanning on separate cohorts of mice at 1, 5, 12, and 18 months. Quantification revealed evident RNFL thickening in the inferior quadrants of the retina (R3 and R4) in Sacs$^{-/-}$ mice compared to Sacs$^{+/+}$ littermates, from 5 months up to 18 months. RNFL size is not increased in R1 and R2 at any of the ages explored (Fig S1), suggesting a spatial specificity of this feature.

We, then, investigated the progression of RNFL thickening in the Sacs$^{-/-}$ mouse model with an OCT longitudinal study, where animals were scanned multiple times, at 1, 3, 5, 7, and 9 months of age (scheme in Fig 1A, B). In parallel, on the same mice, we performed behavioral motor assessments with the BW test at 4 timepoints (1, 3, 5, and 7 months).

RNFL thickening is not detectable at 1 month (indicating that it is not congenital), but in R3 and R4 becomes detectable in the third month and increases up to the seventh month when it becomes stable. Remarkably, RNFL thickening occurs at the same age when Sacs$^{-/-}$ mice show significant motor impairment in the beam walking test, which further worsened at 5 and at 7 months (at this timepoint to a greater extent in males vs females) (Fig 1C, D).

### Thinning of the Corpus Callosum in Sacs$^{-/-}$ Mice

Longitudinal MRI data, with scans obtained at 3 and 9 months of age (Figs 2A and S2), showed a selective thinning of the genu of the *corpus callosum* in Sacs$^{-/-}$ compared to Sacs$^{+/+}$ littermates at both timepoints, whereas the *splenium* showed a significant thinning exclusively at 9 months (see Fig 2B). This significant involvement of the corpus callosum in Sacs$^{-/-}$ mice is in line with the features of white matter involvement recently reported in ARSACS patients.[22] No differences between genotypes were appreciated when evaluating brain or cerebellar indices of atrophy (see Fig 2C, D).

### Sacs$^{-/-}$ Mice Show Mild RGCs Dysfunction

The molecular mechanisms underlying RNFL thickening in ARSACS remain unknown nowadays. Two possibilities may be an increased number of RGCs or enlarged axons.

FIGURE 1: Retinal nerve fiber layer (RNFL) thickening occurs concomitantly and progresses with motor impairment in Sacs$^{-/-}$ mice. (A) Schematic representation of the longitudinal evaluation carried out on Sacs$^{+/+}$ and Sacs$^{-/-}$ mice, created with Biorender.com. (B) Representative optical coherence tomography (OCT) images of the 4 subdivisions (2 superior and 2 inferior) scanned for each eye of Sacs$^{+/+}$ and Sacs$^{-/-}$ mice. The retina was divided using the optic nerve head (ONH) as a marker. Eyes were scanned in a counterclockwise manner starting from the nasal superior quadrant. (C) RNFL thickness of retinal quadrants in Sacs$^{+/+}$ and Sacs$^{-/-}$ mice measured repeatedly every 2 months. Bars represent mean ± standard error of the mean (SEM); n = 8 Sacs$^{+/+}$ and 9 Sacs$^{-/-}$ mice per scan session. Mixed model repeated measure two-way analysis of variance (ANOVA) followed by Sidak's multiple comparisons test: **$P < 0.01$, ***$P < 0.001$, ****$P < 0.0001$. (D) Beam Walking (BW) test performance of Sacs$^{+/+}$ and Sacs$^{-/-}$ mice at 1, 3, 5, and 7 months of age on the same mice analyzed in B. Latency time to cross the beam (left panel) and number of hindfoot missteps (right panel). Bars represent mean ± SEM. One, 3, and 5 months analysis: mixed model repeated measure 2-way ANOVA followed by Sidak's multiple comparisons test: *$P < 0.05$, ***$P < 0.001$, ****$P < 0.0001$; 7 months analysis: 2-way ANOVA followed by Tukey's multiple comparisons test: *$P < 0.05$, **$P < 0.01$, ****$P < 0.0001$. ERG, electroretinography; VEP, visual evoked potential.
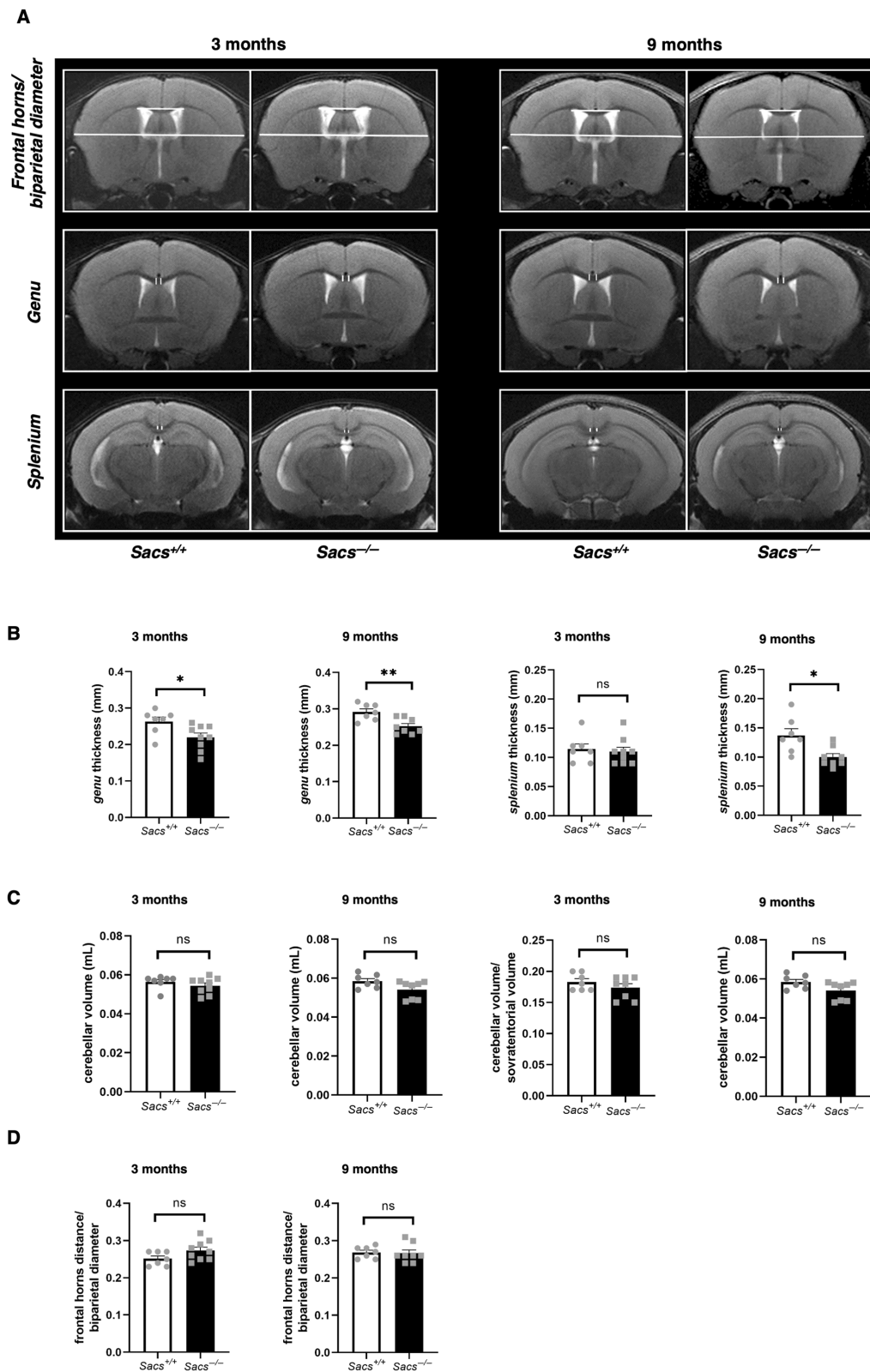
FIGURE 2: *Corpus callosum* involvement in 3- and 9-month-old *Sacs*$^{-/-}$ mice. (A) Representative T2-weighted MRI images showing the linear measures of brains of 3- (left) and 9-month-old (right) mice used for the analyses. In the upper row are shown the biventricular diameter (shorter white line) and the bifrontal diameter used for normalization purposes (longer white line). The 2 lines traced to calculate the mean thickness of genu and the *splenium* of corpus callosum are shown in the middle and lower row, respectively. (B–D) Quantitative analysis of corpus callosum thickness (B), cerebellar volume (C), cortical atrophy (D) in 3- and 9-month-old *Sacs*$^{+/+}$ and *Sacs*$^{-/-}$ mice. Bars represent mean ± standard error of the mean; n = 7 *Sacs*$^{+/+}$ and 9 *Sacs*$^{-/-}$ mice; unpaired 2-tailed *t* test: *$P < 0.05$, **$P < 0.01$.
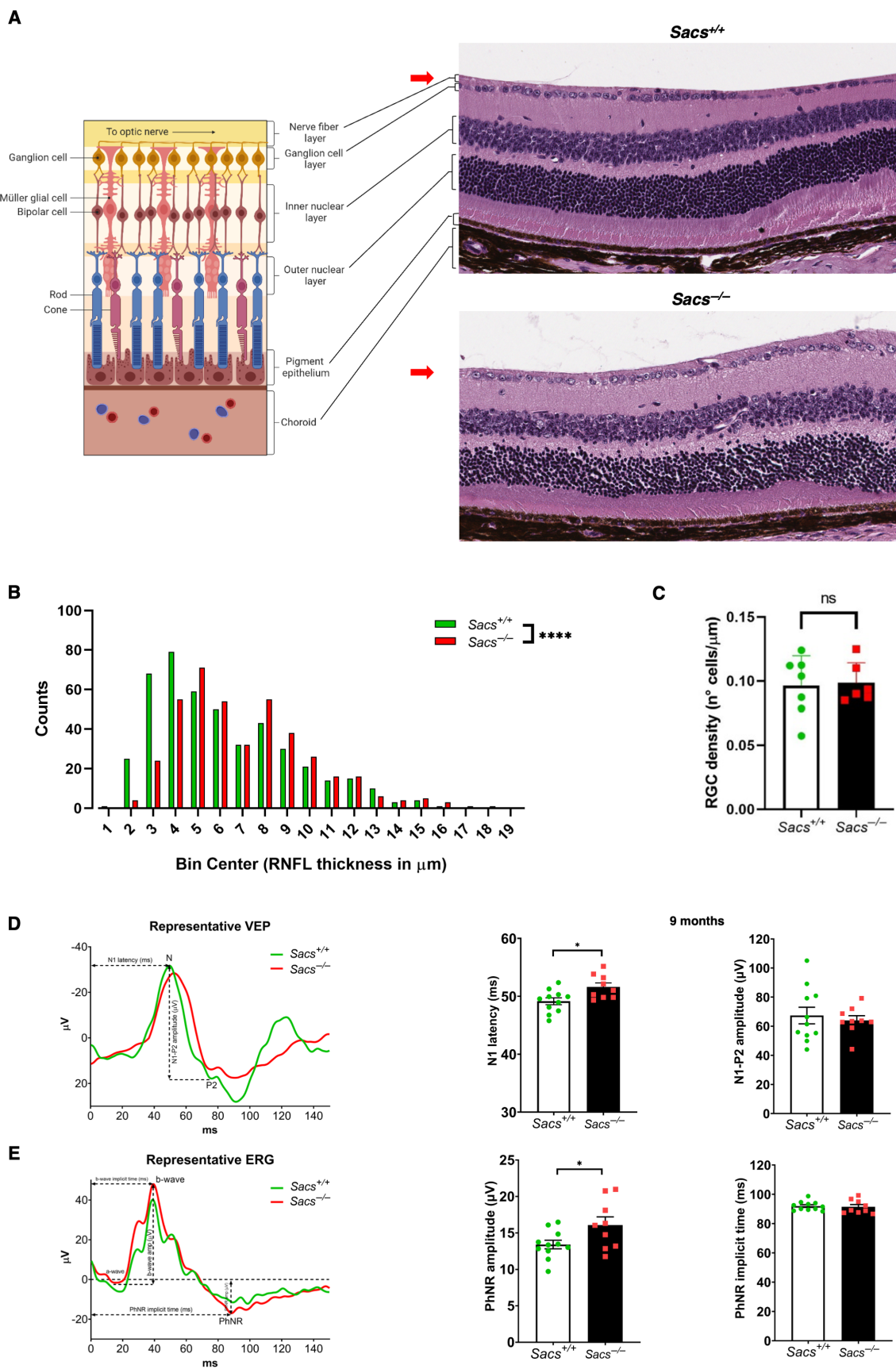
(Figure legend continues on next page.)

H&E staining on retinal slices of 9-month-old mice (Fig 3A), confirmed RNFL thickening in the inferior quadrants of the retina in $Sacs^{-/-}$ mice (see Fig 3B) and revealed a comparable average density of RGC bodies/μm (see Fig 3C).

Retinal function and optic nerve transmission were also assessed by pERG and VEP recordings in 9-month-old mice. Slight but statistically significant increases in the VEP N1 latency of $Sacs^{-/-}$ mice, in photopic negative response (PhNR) (see Fig 3D, E) and b-wave amplitudes (Fig S3B) were detected, implying that a mild myelin pathology and altered retinal responses to the light stimulus are detected at this age. Recordings at 7 months did not reveal such alterations (Fig S3A, B).

RNFL in Sacs$^{-/-}$ Mice Show Increased npNFH and GFAP Reactivity

$Sacs^{-/-}$ mice show early accumulation of npNFH in cerebellar PCs[6,8] and increased GFAP levels, indicative of reactive astrogliosis.[8] We demonstrated that $Sacs^{-/-}$ mice have higher npNFH and GFAP staining intensity in the RNFL as well (Fig 4A, B, see Methods S1 and Fig S4), further supported by increased levels of these proteins by Western blot (WB) analysis performed on retinas (see Fig 4C). Müller glia was not augmented in $Sacs^{-/-}$ retinas, as shown by comparable levels of CRALBP (Fig S5).

Sacs$^{-/-}$ Optic Nerves Display Aberrant Accumulation of NFs

EM of transverse sections of the optic nerves in 9-month-old mice confirmed accumulation of NFs forming multiple dense bundles in $Sacs^{-/-}$ axons and revealed aberrant distribution of microtubules, and appearing displaced to the periphery of the axons (see Fig 4D). WB analysis also showed increased NFH levels in $Sacs^{-/-}$ optic nerves. Axon density within the optic nerve is unaltered in ARSACS mice consistent with the unaltered number of RGCs. An increase in VEP N1 latency could be because of myelin alterations. In agreement, we detected a significant increase in G-ratio values in axons of a specific size (see Figs 4E and S6A, B, C).

Discussion

Here, we demonstrate that both RNFL thickening and MRI parameters change over time in the $Sacs^{-/-}$ mouse model. In detail, RNFL in OCT increases gradually at early phases of pathology (3–5 months), mirroring motor impairment progression to plateau later (7–9 months). We also detected an early thinning of the *genu* of the *corpus callosum*, whereas thinning of its *splenium* becomes detectable over time. We uncovered a mild increase in VEP latency at 9 months likely because of myelin involvement, and an altered responsiveness of RGCs to a light stimulus and indicated by the increased PhNR and b-wave amplitudes in pERG recordings. Mechanistically, RNFL thickening is not because of a higher number of RGCs, but it is rather associated with aberrant accumulation of npNFH and GFAP.

To our knowledge, this is the first report of a retinal phenotype in the $Sacs^{-/-}$ mouse. The restriction of the alterations to the inferior retinal quadrants may be because of a different distribution of RGCs subtypes in the mouse retina, or to species-specificity between human and mouse. Whether ARSACS patients are born with thickened RNFL is debated.[12,23] Our study indicates that it is an acquired feature arising along development. At 1 month of age, RNFL is comparable between $Sacs^{+/+}$ and $Sacs^{-/-}$ mice in OCT. Later, $Sacs^{-/-}$ RNFL thickens, and this feature parallels the insurgence of the motor deficits. The difference between $Sacs^{-/-}$ and $Sacs^{+/+}$ augments regularly up to 5 to 7 months of age, and reaches a plateau, which corroborates what has been described in a small cohort of fully symptomatic patients that did not show further RNFL thickening at a 5-year follow up OCT.[12] Our results may also explain why RNFL thickness in ARSACS patients correlates with age at onset of disease rather than biological age.[11,12]

Although with some restricted exceptions reporting abnormal retinal functionality parameters and even retinal degeneration in ARSACS,[23,24] normally patients do not show peculiar visual alterations, at least in standard ophthalmic tests,[11,12] even in the presence of photoreceptor dysfunction.[25] Our VEP and pERG data highlight that

FIGURE 3: Mild visual alterations in $Sacs^{-/-}$ mice. (A) Schematic representation of the retinal microanatomy with the main retinal layers (left) (created with Biorender.com) and representative hematoxylin–eosin (H&E) staining of 9-month-old $Sacs^{+/+}$ and $Sacs^{-/-}$ mice retina sections (right). Red arrows indicate the retinal nerve fiber layer (RNFL). (B) Distribution of RNFL thickness values and (C) retinal ganglion cell (RGC) density on H&E stained 9-month-old $Sacs^{+/+}$ and $Sacs^{-/-}$ mice retinal sections. We repeatedly sampled the inferior quadrants of the retina from the optic nerve emergence up to 540μm on each side. Bars represent number of events per bin of thickness and mean ± standard error of the mean (SEM) of RGC density; n = 7 $Sacs^{+/+}$ and 6 $Sacs^{-/-}$ mice; Kolmogorov–Smirnov test and unpaired 2-tailed *t* test, respectively: ****$P < 0.0001$. (D) Representative visual evoked potential (VEP) and (E) photopic electroretinography (pERG) profiles of 9-month-old $Sacs^{+/+}$ and $Sacs^{-/-}$ mice with relative quantitation. An increased VEP latency and an augmented photopic negative response (PhNR) amplitude in pERG were detected between genotypes on light stimulation. Bars represent mean ± SEM; n = 11 $Sacs^{+/+}$ and 9 $Sacs^{-/-}$ mice. Unpaired 2-tailed *t* test, *$P < 0.05$.

A Sacs+/+   Sacs−/−

B npNFH   GFAP

C

D Sacs+/+   Sacs−/−

E
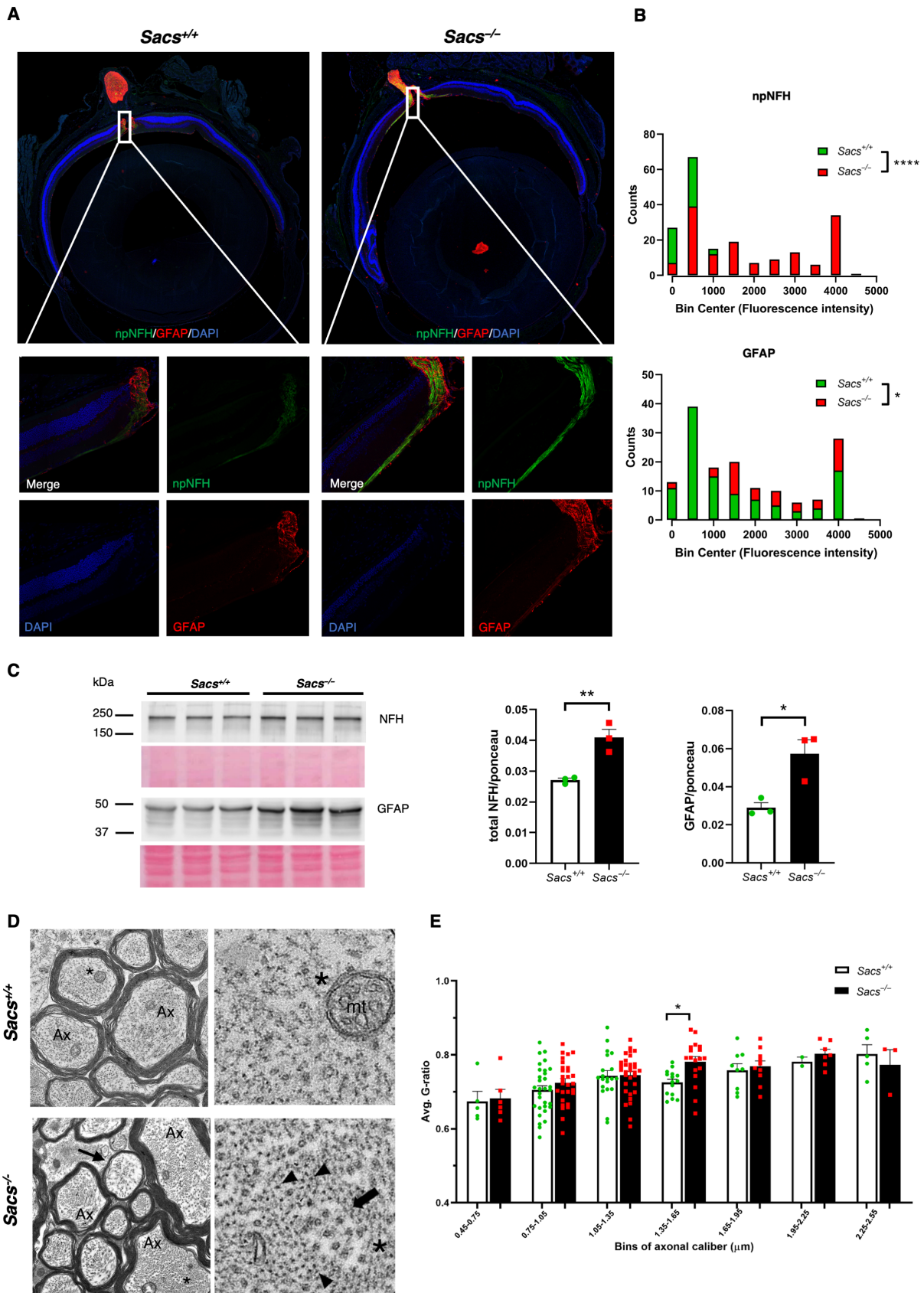
(Figure legend continues on next page.)

some level of retinal dysfunction is present in 9-month-old $Sacs^{-/-}$ mice in response to light stimulation. The same assessments in 7-month-old $Sacs^{-/-}$ mice did not highlight functional alterations, suggesting that they appear at later stages, although specific longitudinal recordings will be needed.

Our data indicate that RNFL thickening is confined to the retina, because $Sacs^{-/-}$ mice present a normal overall structure of the optic nerve, where no difference in axonal density was detected. This suggests that some factors outside of the retina, for example, myelinization and/or limited space allowance, could impede the expansion of $Sacs^{-/-}$ RGC axons. The increased latency in the VEP recordings suggests that alterations in the myelin sheath may be present in $Sacs^{-/-}$ mice, however, investigation of G-ratio values highlighted a defect only in axons of a very restricted axonal diameter range. VEPs are not routinely recorded in patients and to our knowledge, impaired optic nerve function in ARSACS has been reported only once in the past.[26] Our data may indicate that myelin defects could arise during disease progression, suggesting that VEPs might represent new potential biomarkers of disease progression worth investigating in future clinical studies.

To be an ideal biomarker, RNFL thickness should function as a proxy of what happens in neurons in the brain. Our molecular studies identified that npNFH and GFAP reactivity was augmented in $Sacs^{-/-}$ RNFL. In the retina, astrocytes are numerous and exert structural functions alongside providing support to neurons and Müller glia.[27] Retinal astrocytes are interspersed in the RNFL, and it is possible that alterations in their shape and activation state may contribute to the thickening. Single cell studies demonstrate that sacsin expression is rather low in astrocytes both in humans and in mice,[17–19] suggesting a reactive astrocytosis, although a direct effect of sacsin absence in these cells cannot be completely ruled out.

We confirmed that, at least from a conventional MRI standpoint, no significant global brain atrophy is usually found in ARSACS. Furthermore, we failed to find significant differences in cerebellar volume at both timepoints in $Sacs^{-/-}$ mice. A possible explanation might rely in a selective involvement of 1 area of the cerebellum (namely, the superior vermis) compared to the remaining portion. Moreover, we found that the genu of the corpus callosum shows a relatively early involvement in the disease, whereas it's more posterior portion (ie, the *splenium*) is significantly affected at later stages. Along with the confirmation of a significant white matter involvement in this condition, this temporal change might suggest that splenial measurements could be used to evaluate pathology progression in later stages of the disease, when RNFL thickening reaches a plateau.

Altogether, these results identify potential non-invasive objectively measurable biomarkers in ARSACS, which could be further explored in clinical settings and therapeutic trials, such as with repurposed drugs or gene therapy. Given the lack of longitudinal reports in ARSACS patients, mainly because of the long-time span required for follow-ups, studies in animal models of the disease are fundamental for translation into the clinics.

Author Contributions

F.M., A.Q., S.C., L.L., and V.G. contributed to the conception and design of the study; V.G., S.H., G.B., P.P., A.S., and V.C. contributed to the acquisition and analysis

FIGURE 4: Augmented retinal nerve fiber layer (RNFL) thickness associates with increased non-phosphorylated neurofilament H (npNFH) and glial fibrillary acidic protein (GFAP) levels in $Sacs^{-/-}$ mice retinas and aberrant neurofilament accumulation in $Sacs^{-/-}$ optic nerves. (A) Representative confocal images (4×) and higher magnification rendering (63×) of paraffin-embedded retinal sections from $Sacs^{+/+}$ and $Sacs^{-/-}$ mice stained with npNFH (*green*) and GFAP (*red*) showing a more intense npNFH and GFAP staining in $Sacs^{-/-}$ retina compared to $Sacs^{+/+}$ controls. (B) Distribution of peaks of fluorescence intensity over 36 samplings for each retina for npNFH (*top*) and GFAP (*bottom*) on immunofluorescence stained 9-months old $Sacs^{+/+}$ and $Sacs^{-/-}$ mice retinal sections. Bars represent the number of events for each intensity interval; n = 3 $Sacs^{+/+}$ and 4 $Sacs^{-/-}$ mice. Kolmogorov–Smirnov test: *$P < 0.05$, ****$P < 0.0001$. (C) Western blot analysis showing levels of NFH and GFAP in $Sacs^{+/+}$ and $Sacs^{-/-}$ retinas at 9 months of age with relative quantitation (normalized to Ponceau). Bars represent mean ± standard error of the mean; n = 3 $Sacs^{+/+}$ and 3 $Sacs^{-/-}$ mice. Unpaired 2-tailed t test: *$P < 0.05$, **$P < 0.01$. (D) Left column: representative electron microscope (EM) images (70,000× magnification) of an optic nerve section from $Sacs^{+/+}$ and $Sacs^{-/-}$ mice (scale bar = 1μm), Right column: representative EM images (150,000× magnification) showing more electron-dense neurofilament network in optic nerve axons from $Sacs^{-/-}$ mice (scale bar = 200nm). Ax, axon; mt, mitochondrion; *, magnified inset; arrow, microtubule bundles; arrow heads, neurofilament bundles. (E) Average G-ratio per bin of axonal diameter in optic nerve sections from $Sacs^{+/+}$ and $Sacs^{-/-}$ mice. n = 3 $Sacs^{+/+}$ and 3 $Sacs^{-/-}$ mice; 2-way ANOVA followed by Sidak's multiple comparisons test: *$P < 0.05$.

of data; F.M., V.G., and G.B. contributed to drafting the text and preparing the figures.

Potential Conflicts of Interest

Nothing to report.

Data availability

All data are available on request.

References

1. Synofzik M, Soehn AS, Gburek-Augustat J, et al. Autosomal recessive spastic ataxia of Charlevoix Saguenay (ARSACS): expanding the genetic, clinical and imaging spectrum. Orphanet J Rare Dis 2013;8:41. https://doi.org/10.1186/1750-1172-8-41 1750-1172-8-41 [pii].

2. Vermeer S, van de Warrenburg BP, Kamsteeg EJ, et al. Arsacs. In: Adam MP, Ardinger HH, Pagon RA, et al., eds. *GeneReviews((R))*, 1993 updated 2020.

3. Xiromerisiou G, Dadouli K, Marogianni C, et al. A novel homozygous SACS mutation identified by whole exome sequencing-genotype phenotype correlations of all published cases. J Mol Neurosci 2020;70:131–141. https://doi.org/10.1007/s12031-019-01410-z.

4. Lariviere R, Sgarioto N, Marquez BT, et al. Sacs R272C missense homozygous mice develop an ataxia phenotype. Mol Brain 2019;12:19. https://doi.org/10.1186/s13041-019-0438-3.

5. Duncan EJ, Lariviere R, Bradshaw TY, et al. Altered organization of the intermediate filament cytoskeleton and relocalization of proteostasis modulators in cells lacking the ataxia protein sacsin. Hum Mol Genet 2017;26:3130–3143. https://doi.org/10.1093/hmg/ddx197.

6. Lariviere R, Gaudet R, Gentil BJ, et al. Sacs knockout mice present pathophysiological defects underlying autosomal recessive spastic ataxia of Charlevoix-Saguenay. Hum Mol Genet 2015;24:727–739. https://doi.org/10.1093/hmg/ddu491 ddu491 [pii].

7. Gentil BJ, Lai GT, Menade M, et al. Sacsin, mutated in the ataxia ARSACS, regulates intermediate filament assembly and dynamics. FASEB J 2019;33:2982–2994. https://doi.org/10.1096/fj.201801556R.

8. Del Bondio A, Longo F, De Ritis D, et al. Restoring calcium homeostasis in Purkinje cells arrests neurodegeneration and neuroinflammation in the ARSACS mouse model. JCI Insight 2023;8:1–19. https://doi.org/10.1172/jci.insight.163576.

9. Gagnon C, Brais B, Lessard I, et al. From motor performance to participation: a quantitative descriptive study in adults with autosomal recessive spastic ataxia of Charlevoix-Saguenay. Orphanet J Rare Dis 2018;13:165. https://doi.org/10.1186/s13023-018-0898-z.

10. Lessard I, Cote I, St-Gelais R, et al. Natural history of autosomal recessive spastic ataxia of Charlevoix-Saguenay: a 4-year longitudinal study. Cerebellum 2024;23:489–501. https://doi.org/10.1007/s12311-023-01558-w.

11. Parkinson MH, Bartmann AP, Clayton LMS, et al. Optical coherence tomography in autosomal recessive spastic ataxia of Charlevoix-Saguenay. Brain, 2018;141:989–999. https://doi.org/10.1093/brain/awy028.

12. Rezende Filho FM, Bremner F, Pedroso JL, et al. Retinal architecture in autosomal recessive spastic ataxia of Charlevoix-Saguenay (ARSACS): insights into disease pathogenesis and biomarkers. Mov Disord 2021;36:2027–2035. https://doi.org/10.1002/mds.28612.

13. Prasad S, Galetta SL. Anatomy and physiology of the afferent visual system. Handb Clin Neurol 2011;102:3–19. https://doi.org/10.1016/B978-0-444-52903-9.00007-8.

14. Cocozza S, Pontillo G, De Michele G, et al. Conventional MRI findings in hereditary degenerative ataxias: a pictorial review. Neuroradiology 2021;63:983–999. https://doi.org/10.1007/s00234-021-02682-2.

15. Scaravilli A, Negroni D, Senatore C, et al. MRI-ARSACS: an imaging index for autosomal recessive spastic ataxia of Charlevoix-Saguenay (ARSACS) identification based on the multicenter PROSPAX study. Mov Disord 2024;39:1343–1351. https://doi.org/10.1002/mds.29871.

16. Prodi E, Grisoli M, Panzeri M, et al. Supratentorial and pontine MRI abnormalities characterize recessive spastic ataxia of Charlevoix-Saguenay. A comprehensive study of an Italian series. Eur J Neurol 2013;20:138–146. https://doi.org/10.1111/j.1468-1331.2012.03815.x.

17. Lukowski SW, Lo CY, Sharov AA, et al. A single-cell transcriptome atlas of the adult human retina. EMBO J 2019;38:e100811. https://doi.org/10.15252/embj.2018100811.

18. Heng JS, Hackett SF, Stein-O'Brien GL, et al. Comprehensive analysis of a mouse model of spontaneous uveoretinitis using single-cell RNA sequencing. Proc Natl Acad Sci U S A 2019;116:26734–26744. https://doi.org/10.1073/pnas.1915571116.

19. Heng JS, Rattner A, Stein-O'Brien GL, et al. Hypoxia tolerance in the Norrin-deficient retina and the chronically hypoxic brain studied at single-cell resolution. Proc Natl Acad Sci U S A 2019;116:9103–9114. https://doi.org/10.1073/pnas.1821122116.

20. Marenna S, Huang SC, Castoldi V, et al. Functional evolution of visual involvement in experimental autoimmune encephalomyelitis. Mult Scler J Exp Transl Clin 2020;6:2055217320963474. https://doi.org/10.1177/2055217320963474.

21. Rossi G, Ordazzo G, Vanni NN, et al. MCT1-dependent energetic failure and neuroinflammation underlie optic nerve degeneration in Wolfram syndrome mice. Elife 2023;12:1–25. https://doi.org/10.7554/eLife.81779.

22. Scaravilli A, Gabusi I, Mari G, et al. An MRI evaluation of white matter involvement in paradigmatic forms of spastic ataxia: results from the multi-center PROSPAX study. J Neurol 2024;271:5468–5477. https://doi.org/10.1007/s00415-024-12505-y.

23. Desserre J, Devos D, Sautiere BG, et al. Thickening of peripapillar retinal fibers for the diagnosis of autosomal recessive spastic ataxia of Charlevoix-Saguenay. Cerebellum 2011;10:758–762. https://doi.org/10.1007/s12311-011-0286-x.

24. Blumkin L, Bradshaw T, Michelson M, et al. Molecular and functional studies of retinal degeneration as a clinical presentation of SACS-related disorder. Eur J Paediatr Neurol 2015;19:472–476. https://doi.org/10.1016/j.ejpn.2015.02.005.

25. Borruat FX, Holder GE, Bremner F. Inner retinal dysfunction in the autosomal recessive spastic ataxia of Charlevoix-Saguenay. Front Neurol 2017;8:523. https://doi.org/10.3389/fneur.2017.00523.

26. Bouchard JP, Richter A, Mathieu J, et al. Autosomal recessive spastic ataxia of Charlevoix-Saguenay. Neuromuscul Disord 1998;8:474–479. https://doi.org/10.1016/s0960-8966(98)00055-8.

27. Cuenca N, Fernandez-Sanchez L, Campello L, et al. Cellular responses following retinal injuries and therapeutic approaches for neurodegenerative diseases. Prog Retin Eye Res 2014;43:17–75. https://doi.org/10.1016/j.preteyeres.2014.07.001.